HHS Public Access

Author manuscript

Kidney Int. Author manuscript; available in PMC 2022 February 08.

Published in final edited form as:

Kidney Int. 2021 January ; 99(1): 173–185. doi:10.1016/j.kint.2020.08.021.

Magnetic resonance imaging accurately tracks kidney pathology and heterogeneity in the transition from acute kidney injury to chronic kidney disease

Jennifer R. Charlton[1], **Yanzhe Xu**[2], **Teresa Wu**[2], **Kim A. deRonde**[1], **Jillian L. Hughes**[3], **Shourik Dutta**[4], **Gavin T. Oxley**[3], **Aleksandra Cwiek**[3], **Helen P. Cathro**[5], **Nathan P. Charlton**[6], **Mark R. Conaway**[7], **Edwin J. Baldelomar**[8], **Neda Parvin**[8], **Kevin M. Bennett**[8]

[1]Department of Pediatrics, Division Nephrology, University of Virginia, Charlottesville, Virginia, USA;

[2]ASU-Mayo Center for Innovative Imaging, School of Computing, Informatics, Decision Systems Engineering, Arizona State University, Tempe, Arizona, USA;

[3]University of Virginia, Charlottesville, Virginia, USA;

[4]School of Medicine, University of Virginia, Charlottesville, Virginia, USA;

[5]Department of Pathology University of Virginia, Charlottesville, Virginia, USA;

[6]Department of Toxicology, University of Virginia, Virginia, Charlottesville, USA;

[7]Division of Translational Research and Applied Statistics Department of Public Health Sciences, University of Virginia, Charlottesville, Virginia, USA;

[8]Department of Radiology, Washington University in St. Louis, St. Louis, Missouri, USA

Abstract

Acute kidney injury (AKI) increases the risk for chronic kidney disease (CKD). However, there are few tools to detect microstructural changes after AKI. Here, cationic ferritin-enhanced magnetic resonance imaging (CFE-MRI) was applied to examine the heterogeneity of kidney pathology in the transition from AKI to CKD. Adult male mice received folic acid followed by cationic ferritin and were euthanized at four days (AKI), four weeks (CKD-4) or 12 weeks (CKD-12). Kidneys were examined by histologic methods and CFE-MRI. In the CKD-4 and CKD-12 groups, glomerular number was reduced and atubular cortical lesions were observed. Apparent glomerular volume was larger in the AKI, CKD-4 and CKD-12 groups compared to

Correspondence: Jennifer R. Charlton, Division of Nephrology, Department of Pediatrics, University of Virginia Children's Hospital, Box 800386, Charlottesville, Virginia 22903 USA. jrc6n@virginia.edu.

AUTHOR CONTRIBUTIONS

All authors have participated in the concept and design and the drafting and revising of the manuscript. All authors have approved the manuscript as submitted.

DISCLOSURE

JRC, TW, and KMB are co-owners of Sindri Technologies, LLC. EJB and KMB are co-owners of XN Biotechnologies, LLC. KMB has a research agreement with Janssen, LLC. KMB is co-owner of Nephrodiagnostics, LLC. All the other authors declared no competing interests.

SUPPLEMENTARY MATERIAL

Supplementary File (Word)

controls. Glomerular hypertrophy occurred with ageing. Interglomerular distance and glomerular density were combined with other MRI metrics to distinguish the AKI and CKD groups from controls. Despite significant heterogeneity, the noninvasive (MRI-based) metrics were as accurate as invasive (histological) metrics at distinguishing AKI and CKD from controls. To assess the toxicity of cationic ferritin in a CKD model, CKD-4 mice received cationic ferritin and were examined one week later. The CKD-4 groups with and without cationic ferritin were similar, except the iron content of the kidney, liver, and spleen was greater in the CKD-4 plus cationic ferritin group. Thus, our study demonstrates the accuracy and safety of CFE-MRI to detect whole kidney pathology allowing for the development of novel biomarkers of kidney disease and providing a foundation for future *in vivo* longitudinal studies in mouse models of AKI and CKD to track nephron fate.

Keywords

cationic ferritin–enhanced MRI; cluster analysis; folic acid; glomerular number; imaging processing; nephron number

Acute kidney injury (AKI) has short- and long-term consequences in adults, children, and neonates.[1–5] Until recently, it was thought that a return to a normal glomerular filtration rate (GFR) after AKI indicated that the patient's risk of developing chronic kidney disease (CKD) had also returned to baseline. However, new evidence of permanent and heterogeneous structural changes following AKI contradict this assertion.[6–8] Investigations of the transition from AKI to CKD are thus limited by a lack of tools to non-invasively monitor these changes.

Human kidneys contain 200,000 to 2.7 million nephrons.[9] The large range in nephron number is present at birth,[10] with considerable loss of nephrons over a lifetime.[11,12] Our knowledge of nephron number and loss is derived from studies at autopsy using unbiased estimates of glomerular number or from larger studies that use glomerular density from a kidney biopsy and cortical volume from imaging.[12–16] A barrier in clinical research is the lack of tools to assess nephron number and thereby stratify patients enrolling in AKI clinical trials. Surrogates for nephron number may not capture a patient's baseline risk for CKD.[17] Serum creatinine is a late marker of renal dysfunction.[18] Therefore, it is not possible to determine whether elevated creatinine at presentation is related to the acute injury or chronic disease.

Although patients cannot be stratified by nephron number, kidney tissue from biopsies can provide a view of the microstructural heterogeneity. Clinical trials such as the Kidney Precision Medicine Project are being developed to interrogate tissue samples from patients with AKI to understand critical pathways and targets for therapies. However, sampling bias[19] and size constraints remain limitations in traditional histologic evaluations. Optical clearing followed by light sheet or confocal microscopy has overcome some of the limitations of biopsy-based histology to provide high-resolution images at depths of >1 mm.[20]

Similar to humans, the severity of AKI, individual response, and histologic manifestations can be highly variable in animal models of AKI. There are several animal models used to study the transition from AKI to CKD, each with merits and pitfalls. For this study, we chose the folic acid model of nephropathy, which develops urinary crystals, tubular obstruction, and direct cellular toxicity in a heterogeneous pattern; variability such as this is often seen with AKI in humans. Our goal was to evaluate the microstructural changes in the transition from AKI to CKD using 3-dimensional (3D) techniques.

Cationic ferritin–enhanced magnetic resonance imaging (CFE-MRI) is a tool to measure glomerular number (N_{glom}) and size (aV_{glom}), allowing for a nondestructive, 3D, whole kidney assessment of perfused nephron number.[21] CFE-MRI has been developed[22–24] to visualize glomeruli and their relation to the other kidney compartments. Cationic ferritin (CF) is formed from ferritin, a highly conserved protein that incorporates iron oxide nanoparticles in its core. The ferritin surface is functionalized with an amine-containing cross-linker,[25] allowing it to bind to anionic sites within the glomerulus. The iron core of ferritin shortens the transverse magnetic resonance relaxation times causing the CF-labeled glomeruli to appear as dark spots in T2*-weighted images. CFE-MRI has been used safely[22,23] *ex vivo* and *in vivo* in rats and mice,[26–29] human kidneys unsuitable for transplant,[30] and in a rabbit model of neonatal AKI.[24] Although the use of CFE-MRI is becoming more widespread, much of the work has focused on healthy animals. There is little information comparing 3D MRI metrics to traditional 2-dimensional histologic assessments or the performance of the 3D MRI metrics to assess whole kidney heterogeneity in kidney disease.

Here, we applied CFE-MRI to examine renal pathology from AKI to CKD in a mouse model of folic acid nephropathy. We mapped structural changes in glomeruli and tubules during CKD progression in 3D (Figure 1) and investigated whether glomerular loss was associated with glomerular hypertrophy. We evaluated the heterogeneity of the microstructural pathology using noninvasive (MRI-based) and invasive (histologic-based) biomarkers. Finally, we determined the safety of CF in the CKD model. This work demonstrates that the metrics derived from CFE-MRI can categorize the AKI and CKD groups as accurately as standard histologic metrics and provide a foundation for longitudinal studies of mouse models of AKI and CKD, *in vivo*, where individual nephrons can be monitored to predict and prevent the progression of CKD over time.

RESULTS

Traditional kidney measurements to track the transition from AKI to CKD

Body weight, GFR, kidney weight to body weight ratio, and histologic scores of AKI severity along with scarred area of the kidneys were measured. Data are displayed in Supplementary Figure S1. The mice lost body weight for the first week after folic acid injection, but returned to their baseline weight by 21 days. At 12 weeks, the group that received folic acid had an average weight of 27.9 g (interquartile range [IQR]: 23.4–29.0 g), whereas the control group weighed 30.1 g (IQR: 28.9–32.1), $P = 0.02$, Supplementary Figure S1A). The median baseline GFR was 211 μl/min (IQR: 174–241 μl/min) and dropped to 105 μl/min (IQR: 79–174 μl/min, $P = 0.007$, Wilcoxon test) 4 days after folic acid was

administered. Four weeks after injury (CKD-4), the median GFR was 169 μl/min (IQR: 145–199 μl/min, $P = 0.25$), and at 12 weeks after injury (CKD-12), the GFR was 186 μl/min (IQR: 123–237 μl/min, $P = 0.81$, Supplementary Figure S1B). The kidney to body weight ratio was significantly greater in the AKI group, but lower in the CKD-12 group compared with their respective control groups (Supplementary Figure S1C). Histologically, the severity of AKI was measured using a scoring system ranging from 0 to 3. The median AKI score for the AKI group was 2, compared to 0 in the controls, Supplementary Figure S1D. In the CKD groups, the trichrome stain was used to measure the area occupied by cortical lesions (Supplementary Figure S1E). The CKD-4 group had a median of 17% of cortex occupied by lesions, whereas the control group had a median of 0% ($P < 0.001$). The CKD-12 group had 11% of the kidney occupied by lesions, and the control group had 0% ($P < 0.001$, Table 1).

Kidney volume was measured by MRI (Table 1). Those with AKI had greater volume than controls. CKD-4 and CKD-12 groups had smaller kidney volumes than their controls. In the controls, the volume of the kidney increased with age (control at 12 weeks: 212 ± 24 mm^3 vs. controls at AKI: 168 ± 17 mm^3, $P = 0.001$).

Insights into the transition between AKI and CKD

Glomerular number is reduced with concurrent glomerular hypertrophy by 4 weeks after folic acid administration.—MRI and histologic metrics are summarized in Table 1. N_{glom} and aV_{glom} were determined by CFE-MRI (Figure 2). In the AKI group, the glomerular basement membrane remained intact, allowing the CF to bind, making it detectable by MRI (Figure 2a and b). N_{glom} was not different between the AKI and control groups (Figure 2g). Median aV_{glom} of the AKI group was statistically greater than in the controls, but the absolute difference between groups was small (Figure 2h).

In the CKD-4 and CKD-12 groups, N_{glom} was significantly lower than in the control groups. Between 4 and 12 weeks after injury, N_{glom} remained stable between the CKD-4 and CKD-12 groups. In the CKD model, there was a variable degree of tubular loss. In these areas, glomeruli were detected; however, they could not be measured due to their close proximity (Figure 2c and d). Therefore, these clustered glomeruli were not included in the aV_{glom} metric. Instead, a new imaging biomarker called a “cortical lesion” was developed (further details below).

Using the complete aV_{glom} dataset from each animal, we found that aV_{glom} from the CKD-4 and CKD-12 groups were greater than their respective control groups (Figure 2h). However, there was a significant increase in aV_{glom} as the animals aged (CKD-12 controls: 1.9 (IQR: 1.6–2.6 × 10^{-4} mm^3) versus AKI controls: 1.6 (IQR: 0.9–1.5 × 10^{-4} mm^3), $P < 0.001$; Mann-Whitney test).

Histologic sections were used to measure the area of the glomeruli inside and outside of the cortical lesions in CKD-4 and CKD-12 groups compared with controls. The area of the glomeruli inside (3.6 ± 1.9 × 10^4 μm^2) was similar to those outside (3.1 ± 1.2 × 10^4 μm^2, $P = 0.16$, t test) the cortical lesions in the CKD-4 group. However, glomeruli inside the lesions were smaller (3.4 ± 1.5 × 10^4 μm^2) than those outside the lesions (4.3 ± 1.6 × 10^4 μm^2, $P = 0.007$) at 12 weeks. The glomeruli outside of the lesions were smaller (4.3 ± 1.6 × 10^4

μm^2) than glomeruli in the control group ($4.8 \pm 1.5 \times 10^4$ μm^2, $P = 0.046$). The glomeruli in the 12-week control group ($4.8 = 1.5 \times 10^4$ μm^2) were larger than in 4-week controls ($3.1 \pm 0.99 \times 10^4$ μm^2, $P < 0.0001$) supporting the observation from MRI that aV_{glom} increases with age.

In summary, the AKI and control groups had similar N_{glom} and aV_{glom}. However, in early CKD (CKD-4), there is a reduction in N_{glom} accompanied by an increase in aV_{glom}. Glomerular hypertrophy occurs over time in both in the healthy animals.

The predominant histologic feature of the AKI group was tubular dilation, and atubular glomeruli were present in both the AKI and CKD groups.—Dilated tubules were more common in the AKI group (Figure 3a–c) than in controls. Collagen deposition was observed in lesions in the kidneys from the CKD-4 and CKD-12 groups stained with trichrome. Glomeruli were present in the cortical lesions but were surrounded by atrophic tubules or, in many cases, lacked tubules (Figure 3d–f). The fraction of lotus-negative glomeruli was significantly greater in the CKD-12 groups compared to age-matched controls (Figure 3g–i). There was no change in the number of lotus-negative glomeruli from aging alone. The proximal tubular fraction was significantly reduced in the CKD-4 and CKD-12 groups compared with controls (Figure 3j–l). In the control group at the time of AKI, the proximal tubular fraction was 46%, compared to 46% in the controls at 12 weeks ($P = 0.02$, *t* test).

Novel AKI MRI metrics: glomerular volume distribution, glomerular density and interglomerular distance.—The distribution of aV_{glom} in the AKI group ($1.78 \pm 0.44 \times 10^{-4}$ mm^3) was statistically significantly different from the control group ($1.75 \pm 0.43 \times 10^{-4}$ mm^3, Figure 4a). There was a lower glomerular density in the whole kidney cortex in mice with AKI compared with controls (Figure 4b, Table 1). Similarly, both the outer and inner cortex of the AKI kidneys had a lower glomerular density than controls (Figure 4b). The median and minimum interglomerular distances (Figure 4c) were similar between the AKI group and controls, and there was no discernable spatial pattern in interglomerular distance, as shown in Figure 4d.

Novel CKD MRI metric: Cortical lesions can be measured by CFE-MRI throughout the whole kidney.—There was a significant difference in the distributions of aV_{glom} in the CKD-4 and CKD-12 groups compared to controls, $P < 0.001$ (Figure 4e and f, Table 1). The number of lesions was significantly higher in the CKD-4 and CKD-12 groups compared with controls. The volume (Figure 4g) and fraction of kidney occupied by lesions were higher in the CKD-12 group. Lesion number, size and fraction of the kidney occupied by the lesions were similar between the CKD-4 and CKD-12 groups.

MRI is as accurate as histology in identifying AKI and CKD

Increased heterogeneity in the AKI and CKD groups compared to controls using a combination of noninvasive (MRI) and invasive (histologic) metrics.—MRI and histologic metrics were analyzed using principal component analysis (PCA). To measure the overall heterogeneity of the folic acid model, the Euclidean distance of the

principal component of any 2 kidneys was calculated within the same group. The average distance between individuals in the AKI group was 1.90, compared with the control group where the average distance was 1.66 (Figure 5a), demonstrating significant heterogeneity in the AKI group. Heterogeneity of the model was also observed in the CKD groups. The average distance between individuals in the CKD-4 group was 2.05 (compared with the controls: 1.13, Figure 6a), and the greatest amount of heterogeneity was in the CKD-12 group where the average distance between individuals was 2.27 (compared with the control group: 0.66, Figure 6d).

Metrics were classified as invasive (mainly histologic) or noninvasive (mainly MRI). See Table 2 for a complete list. We found a greater distance between the individual data points and the cluster center in the experimental groups compared to the control groups, indicating significant heterogeneity in the experimental groups assessed by either noninvasive or invasive metrics.

The cluster centers did not overlap between any of the compared groups, suggesting that these metrics could discriminate between the experimental groups (AKI and CKD) and the control group. For the noninvasive MRI metrics, the cluster center of the AKI group (coordinates: 1.9, 0.15) was distinct from the control group (coordinates: −1.69, 0.14, $P = 0.001$, Figure 5b). There was also a significant difference in the cluster center of the noninvasive metrics for the CKD-4 and CKD-12 groups: CKD-4 (2.32, 0) and control (−1.8, 0), $P = 0.001$; CKD-12 (2.17, 0.04) and control (−1.93, 0.03), $P = 0.001$ (Figure 6b and e).

Misclassification of AKI or CKD by noninvasive (MRI) metrics and invasive (histologic) metrics.—None of the animals in the control groups were misclassified in an experimental group. However, several experimental animals were classified as controls, likely representing a mild disease phenotype. In the AKI group, 3 animals (648, 650, 655) clustered with the controls by invasive metrics (Figure 5c), and a single animal (433) was clustered with the controls by noninvasive metrics, Figure 5b. CKD animal 616 classified as a control based on both invasive and noninvasive metrics (Figure 6b and c). In the CKD-12 cohort, CKD animals 602, 5976, and 5974 were classified as controls on the invasive, and 603 was classified at a control on the noninvasive metrics (Figure 6b and c). Noninvasive (MRI) metrics captured the heterogeneity within the AKI, CKD-4, and CKD-12 groups and also distinguished the diseased kidneys from the healthy ones as well as, if not more accurately, than the invasive (histologic) metrics.

Metrics that contribute the greatest to discrimination between diseased and healthy kidneys.—The individual contribution of each of the metrics to the PCA is shown in Supplementary Tables S1–S3. Kidney to body weight and tubular dilation contributed the most to differentiating the AKI group from controls (Supplementary Table S1). The largest contributions to the clustering of the CKD-4 group were from atubular glomeruli and cortical lesion volume (Supplementary Table S2). The CKD-12 group was distinguished controls by N_{glom} and median aV_{glom} (Supplementary Table S3).

Cationic ferritin is not toxic in the CKD model

CF toxicity was assessed in the CKD model at 4 weeks (Supplementary Figure S2). The body weights of the CKD-4 with CF and without CF were similar at the time of euthanasia (CKD-4+CF: 24.5, IQR: 24.4–25.9), CKD-4 without CF: 28.3, IQR: 23.1–28.4), $P = 0.68$). There was no iron or ferritin detected by histology in the kidneys. In the CKD+CF group, iron was located in the Kupffer cells and ferritin in the hepatocytes of the liver, and both were located in the red pulp of the spleen. Kidney, liver, or spleen weight (normalized to body weight) was similar between CF-injected mice and controls. The median nonheme iron content of the kidney, liver, and spleen was higher in the group that received CF. White blood counts, hemoglobin, or platelets were similar between the groups. Serum iron levels were also similar (CKD-4+CF: 134, IQR: 92–135), CKD-4 without CF: 117 mcg/dl, IQR: 106–128, $P = 0.80$). Renal function assessed by creatinine was comparable between the groups (CKD-4+CF: .2 mg/dl, CKD-4 without CF: 0.2, $P = 1.0$). Liver function measured by aspartate transaminase (AST) and alanine transaminase (AST) was similar between the group that recent CF and those that did not receive CF.

DISCUSSION

In this work, we tracked the transition from AKI to CKD using CFE-MRI and histology. The predominant features of the model were a focal loss of tubules and a reduction in the number of glomeruli. This allowed for the development of a new imaging biomarker, termed cortical lesions. With a decrease in glomerular number, aV_{glom} increased. We observed glomerular hypertrophy over time in the healthy controls. Finally, we observed that CFE-MRI metrics could discriminate AKI and CKD from healthy mice as accurately as histologic metrics, and with fewer misclassifications. We conclude that (i) CFE-MRI can detect atubular cortical lesions and glomerular hypertrophy, (ii) noninvasive metrics derived from CFE-MRI can be used to differentiate AKI and CKD after folic acid tubular injury, and (iii) atubular glomeruli were a prominent feature in this model of CKD. The remaining intact glomeruli increased in size over time with a reduced proximal tubular mass. Regions of atubular glomeruli (ATG) were detected by CFE-MRI as collections of glomeruli that were not separated by tubules, termed cortical lesions by CFE-MRI. The disconnection of the glomerular tubular junction is a common but often undetected response to kidney injury.[31] ATG are seen in humans and rodent models of CKD.[32–38] The ATG were smaller than those with an intact glomerular–tubular junction outside the lesions. Contrary to a recent study in a rabbit model of neonatal AKI,[24] these glomeruli maintain blood flow and were labeled by CF, suggesting an intact GBM. This contradiction may reflect a difference in the species, timing of injury, or mechanism of injury. In this folic acid–induced AKI model, the size of the cortical lesions or proportion of atubular glomeruli was similar between early and late CKD. By MRI, the cortical lesion size and number was similar between the CKD-4 and CKD-12 groups and the percentage of ATG was the same in the CKD-4 and CKD-12 groups. Further work is necessary to determine the function of ATG, including their possible role in regulating hydrostatic pressure in the surviving nephrons or in maintenance of endocrine function.

In future work, we will apply CFE-MRI *in vivo* to track individual nephrons through injury to recovery or termination. A benefit of CFE-MRI is that each functional

glomerulus provides an “anchor” to develop novel metrics such as glomerular density and interglomerular distance and small changes can be detected, such as the increase in glomerular size in the AKI group compared to controls. However, these small differences must be interpreted cautiously, and *in vivo* validation is required to ensure these metrics are physiologically meaningful. This work provides the foundation to develop longitudinal, repeatable imaging biomarkers to detect early changes in glomerular microstructure following AKI and progression to CKD. Other compartments of the kidney can also be targeted and evaluated by MRI with other contrast techniques. For example, it may be possible to integrate this type of work with new approaches to detecting fibrosis[39,40] or integrate the glomerular and vascular pathology.[41]

The response to folic acid in the mouse is highly variable,[42] consistent with the variations in severity and outcomes of human AKI. The clustering analysis here reflects the heterogeneity in this model. The AKI group was distinguished from controls, but there was significantly more variability in AKI and CKD groups compared to controls in both the MRI and histologic metrics. A strength of this study was use of PCA to discriminate the heterogenous experimental groups and their respective controls using either histologic or MRI metrics or a combination of both metrics. Heterogeneity in glomerular structure is not a new concept.[43] In 1842, William Bowman discovered that glomeruli deeper in the kidney were larger than the superficial glomeruli, which has been confirmed in many species.[44] Variability is not limited to the glomeruli; the efferent arterioles of the juxtamedullary glomeruli are larger, and the loops of Henle are longer.[45] Furthermore, rats, mice, and chinchilla exhibit intrarenal heterogeneity in single-nephron GFR.[46–48] Despite the heterogeneity in the model, animals were more likely to be classified into their experimental group using the MRI metrics than by using the histologic metrics. This suggests that with future studies, animals can potentially be stratified by degree of injury in therapeutic drug trials, increasing the sensitivity to detect a change. With CFE-MRI, we can now examine heterogeneity at the level of the whole organ and eventually combine this knowledge with molecular and physiologic data to form a comprehensive view of renal health and disease.

To address the concern for toxicity in CFE-MRI, we screen for any adverse effects of CF in each new model.[22–24] Consistent with previous work,[22] the animals that received CF had a transient period of weight loss, but after a week, body or organ weight were similar between the groups. As expected, there was a higher concentration of iron in the kidney, liver, and spleen in the CKD-4+CF group; however, the groups had similar kidney or liver function.

In conclusion, CFE-MRI provides novel insights into the transition from AKI to CKD, including whole kidney glomerular number, size, distance, and tubular loss. CFE-MRI metrics capture heterogeneity within the kidney and characterize kidney pathology at least as accurately as histologic metrics, and possibly with fewer misclassifications. This study demonstrates the accuracy and safety of CFE-MRI to detect whole kidney pathology, providing a foundation for future *in vivo* longitudinal studies of mouse models of AKI and CKD to track nephron fate and predict and prevent the progression of CKD.

MATERIALS AND METHODS

Animal experiments were approved by the Institutional Animal Care and Use Committee at the University of Virginia, in accordance with the National Institutes of Health Guide for the Care and Use of Laboratory Animals. Adult male C57Bl/6 mice were purchased from Jackson Laboratory (Bar Harbor, ME) or bred at the University of Virginia. Animals received i.p. folic acid in 0.3 $NaHCO_3$ (125 mg/kg body weight, n = 20) or 0.3 M $NaHCO_3$ (n = 16) at 9 to 11 weeks. After folic acid, the mice were given 10 to 20 ml/kg of 0.9% NaCl subcutaneously for volume resuscitation. The mice were euthanized after the folic acid at 4 days (AKI, n = 9; control n = 8), 4 weeks (CKD-4, n = 8; control, n = 8), or 12 weeks (CKD-12, n = 9; control, n = 8).

On the day of euthanasia, each mouse received horse spleen CF (5.75 mg/100 g body weight; F7879, Sigma Aldrich, St. Louis, MO) in 2 tail vein injections 90 minutes apart and euthanized 90 minutes after the final injection (tribromoethanol solution, i.p. and intra-cardiac perfusion). Horse spleen CF is a combination of heavy and light chains. A kidney from each animal was placed in a custom plastic device holding up to 8 kidneys for MR imaging. A Bruker 7T/30 MRI (Bruker, Co., Billerica, MA) with a quadrature RF probe (inner diameter = 30 mm) and Siemens software were used for acquisition and reconstruction (Siemens, Munich, Germany). Images were acquired using a 3D T2*-weighted pulse sequence with echo time and repetition time of 20/80 ms, slice thickness = 60 μm, field of view 26 mm, matrix size = 640 × 640 × 256 and in plane spatial resolution 41 × 41 × 60 μm^3.

Image processing and measurement of the MRI biomarkers were performed using Fiji,[49] Matlab (The Mathworks, Natick, MA), and Python (Python Software Foundation, https://www.python.org/). Each kidney was segmented from the original magnetic resonance images (8 kidneys/scan), and the cortex was isolated from the medulla.

Glomerular number (N_{glom}) and apparent glomerular volume (aV_{glom}) were calculated from the segmented cortex images. A difference of gaussian filter with an optimal scale ($t^* = 1$)[50] was applied to reduce image noise. Next, a 3D Hessian map was constructed to identify candidate glomeruli. Simultaneously U-Net, a deep learning model, was applied to the same image in 3D. The U-Net model produced a probability map for each voxel to belong to a glomerulus. A probability threshold of 0.5 was applied to identify candidate glomeruli. The Hessian and probability maps were then joined to identify "true" glomeruli.[50] Finally, the individual glomeruli were counted using the Connected Component algorithm in Matlab. The renal cortex was divided into an inner and outer region to provide regional assessments of several MRI metric described below. Individual glomerular volumes were calculated using line profiles drawn through each identified glomerulus, as previously described.[28] The glomerular diameter was defined by the 20% of the profile height to compute aV_{glom}. We performed quality control by reiterative visual inspection of the images.

MRI biomarker analysis of the AKI group

Interglomerular distance and glomerular density were measured in the cortex. The interglomerular distance was the average distance from each glomerulus to neighboring

glomeruli, limited to 250 μm. Interglomerular distance was limited to avoid sampling across large distances where glomeruli were not located, such as across the medulla. To derive the average glomerular density, 100 cubes in 16 × 16 × 16 voxels (1.0×10^5 μm^3/voxel) were randomly distributed throughout the cortex of each kidney (defined as the number of glomeruli inside the cube divided by the volume of the cube). The same procedure was conducted 5 times in each kidney to remove sampling bias because regions were randomly selected. We conducted analysis of variance and concluded the 100 samples from each run had consistent measures indicating 5 runs were sufficient to address the sampling bias.

Glomerular density was measured throughout the kidney and regionally in the outer and inner cortex but the size of the sampling cube was reduced to 10 × 10 × 10 voxels (1.0×10^5 μm^3/voxel) in inner and outer cortex. Again, 100 cubes were used and the measurement was repeated 5 times.

MRI biomarker analysis of the CKD groups

MR images revealed CF-labeled glomeruli in the cortex that were located closely adjacent to each other where the glomeruli were “clustered” together (Figure 1). To distinguish this from the clustering analysis (described subsequently), these areas are hereafter called cortical “lesions.” A cortical lesion was defined by an area of CF labeling that was larger than any individual glomerulus. We calculated the distance of any voxel to its boundary in the larger regions identified as lesions and applied an unsupervised clustering algorithm, Density-Based Spatial Clustering of Applications with Noise (DBSCAN)[51] to estimate the number and volume of lesions. N_{glom} and aV_{glom} were measured outside the lesions.

Histologic assessments

The contralateral kidney was prepared for histologic assessment by formalin immersion fixation and paraffin embedment. Sections were cut at a thickness of 4 μm and an AKI score,[52] proximal tubular fraction,[31,53] atubular glomeruli (%),[54,55] and scarred area (%) were calculated from a periodic acid–Schiff, lotus lectin, and trichrome stains. Details of metrics are described in detail in the supplementary materials.

Kidney clustering analysis

We performed PCA to determine the heterogeneity in each group and compare MRI metrics to histology.[56,57] PCA was used because it reduces redundant information from highly correlated metrics, and individual contributions from the raw variables can be assessed. The MRI and histologic metrics were classified as invasive or noninvasive (Table 2). SCREE plots are available in Supplementary Figure S3. All metrics were normalized to a scale from 0 to 1. In most cases, the inflection point of the SCREE plots was between 2 and 3. Therefore, the k-means clustering analysis (k = 2) was conducted using the first and second PC for 3 groups (AKI, CKD-4, and CKD-12). Three clustering analyses were conducted on invasive metrics, noninvasive metrics, and a combination of the invasive and noninvasive metrics.

Toxicology of horse spleen CF

The CKD-4 model alone was used for toxicity assessment. This was considered justified to avoid duplicative animal studies because the CKD-4 and CKD-12 groups were similar other than aV_{glom}, which was also different in the controls. A PCA was conducted to compare the CKD-4 to CKD-12 groups, and the groups could not be distinguished (Supplementary Figure S4). Adult male mice received folic acid at 9 to 11 weeks. Four weeks after injury, the mice received CF at 5.75 mg/100 g body weight. The mice were monitored for 1 week then euthanized with a blood collection for a complete blood count, comprehensive metabolic panel, and iron level using the University of Virginia medical laboratory. Kidneys, livers, and spleens were paraffin embedded to determine the location of iron using Perls's Prussian blue stain and ferritin using immunohistochemistry. Details of these procedure are included in the supplementary materials and have been published previously.[22] A portion of each organ was used to measure iron content.[58,59]

Statistical analysis

With 8 animals per group, the 2-sample *t* test has 80% power with a 2-sided significance level of 5% for an effect size of 1.5. The data in Baldelomar *et al.*[28] suggest that 1.5 is a conservative estimate of the effect size because the reported estimated effect sizes were 6.9, 4.5, and 6.6 based on MRI, stereology or acid maceration, respectively. For comparing V_{glom}, the estimated effect sizes were 1.7 and 2.7 using MRI and stereology.

The Anderson–Darling test was used to determine the normality of the data. Normally distributed data were reported as means and standard deviations. Nonnormally distributed data were reported by median and interquartile ranges. Two sample Student's *t* test was applied to compare the means of normal data. The Mann–Whitney test was applied for nonparametric analyses and paired data was compared by Wilcoxon test. A Bonferroni correction was applied, and P values < 0.002 were considered statistically significant. The energy test,[60] a multivariate nonparametric test, was applied to kidney clustering analysis to compare the cluster centers.

Supplementary Material

Refer to Web version on PubMed Central for supplementary material.

ACKNOWLEDGMENTS

JRC, TW, and KMB are funded by the National Institutes of Health (NIH)/National Institute of Diabetes and Digestive and Kidney Diseases: R01DK111861 and R01DK110622. JRC is funded by 1U34DK117128. This work used the Bruker ClinScan 7T MRI in the Molecular Imaging Core, which was purchased with support from NIH grant 1S10RR019911-01 and is supported by the University of Virginia School of Medicine.

The authors acknowledge the expertise of Rene "Jack" Roy in the Molecular Imaging Core at the University of Virginia and Jeremy Gatesman in the Center for Comparative Medicine.

REFERENCES

1. Heung M, Chawla LS. Acute kidney injury: gateway to chronic kidney disease. Nephron Clin Pract. 2014;127:30–34. [PubMed: 25343817]

2. Mammen C, Al Abbas A, Skippen P, et al. Long-term risk of CKD in children surviving episodes of acute kidney injury in the intensive care unit: a prospective cohort study. Am J Kidney Dis. 2012;59:523–530. [PubMed: 22206744]

3. Chaturvedi S, Ng KH, Mammen C. The path to chronic kidney disease following acute kidney injury: a neonatal perspective. Pediatr Nephrol. 2017;32:227–241. [PubMed: 26809804]

4. Zwiers AJ, Ijsselstijn H, van Rosmalen J, et al. CKD and hypertension during long-term follow-up in children and adolescents previously treated with extracorporeal membrane oxygenation. Clin J Am Soc Nephrol. 2014;9:2070–2078. [PubMed: 25278545]

5. Harer MW, Pope CF, Conaway MR, et al. Follow-up of Acute kidney injury in Neonates during Childhood Years (FANCY): a prospective cohort study. Pediatr Nephrol. 2017;32:1067–1076. [PubMed: 28255805]

6. Venkatachalam MA, Griffin KA, Lan R, et al. Acute kidney injury: a springboard for progression in chronic kidney disease. Am J Physiol Renal Physiol. 2010;298:F1078–F1094. [PubMed: 20200097]

7. Basile DP. The endothelial cell in ischemic acute kidney injury: implications for acute and chronic function. Kidney Int. 2007;72:151–156. [PubMed: 17495858]

8. Choi YJ, Chakraborty S, Nguyen V, et al. Peritubular capillary loss is associated with chronic tubulointerstitial injury in human kidney: altered expression of vascular endothelial growth factor. Hum Pathol. 2000;31: 1491–1497. [PubMed: 11150374]

9. Bertram JF, Douglas-Denton RN, Diouf B, et al. Human nephron number: implications for health and disease. Pediatr Nephrol. 2011;26:1529–1533. [PubMed: 21604189]

10. Zhang Z, Quinlan J, Hoy W, et al. A common RET variant is associated with reduced newborn kidney size and function. J Am Soc Nephrol. 2008;19:2027–2034. [PubMed: 18820179]

11. Nyengaard JR, Bendtsen TF. Glomerular number and size in relation to age, kidney weight, and body surface in normal man. Ana Rec. 1992;232: 194–201.

12. Denic A, Lieske JC, Chakkera HA, et al. The substantial loss of nephrons in healthy human kidneys with aging. J Am Soc Nephrol. 2017;28:313–320. [PubMed: 27401688]

13. Denic A, Mathew J, Lerman LO, et al. Single-nephron glomerular filtration rate in healthy adults. New Engl J Med. 2017;376:2349–2357. [PubMed: 28614683]

14. Sasaki T, Tsuboi N, Okabayashi Y, et al. Estimation of nephron number in living humans by combining unenhanced computed tomography with biopsy-based stereology. Sci Rep. 2019;9:14400. [PubMed: 31591408]

15. Lenihan CR, Busque S, Derby G, et al. Longitudinal study of living kidney donor glomerular dynamics after nephrectomy. J Clin Invest. 2015;125: 1311–1318. [PubMed: 25689253]

16. Lenihan CR, Busque S, Derby G, et al. The association of predonation hypertension with glomerular function and number in older living kidney donors. J Am Soc Nephrol. 2015;26:1261–1267. [PubMed: 25525178]

17. Denic A, Elsherbiny H, Rule AD. In-vivo techniques for determining nephron number. Curr Opin Nephrol Hypertens. 2019;28:545–551. [PubMed: 31433316]

18. Moran SM, Myers BD. Course of acute renal failure studied by a model of creatinine kinetics. Kidney Int. 1985;27:928–937. [PubMed: 4021321]

19. Waikar SS, McMahon GM. Expanding the role for kidney biopsies in acute kidney injury. Semin Nephrol. 2018;38:12–20. [PubMed: 29291757]

20. Krolewski DM, Kumar V, Martin B, et al. Quantitative validation of immunofluorescence and lectin staining using reduced CLARITY acrylamide formulations. Brain Struct Funct. 2018;223:987–999. [PubMed: 29243106]

21. Bennett KM, Zhou H, Sumner JP, et al. MRI of the basement membrane using charged nanoparticles as contrast agents. Magn Reson Med. 2008;60:564–574. [PubMed: 18727041]

22. Charlton JR, Pearl VM, Denotti AR, et al. Biocompatibility of ferritin-based nanoparticles as targeted MRI contrast agents. Nanomedicine. 2016;12: 1735–1745. [PubMed: 27071333]

23. Beeman SC, Georges JF, Bennett KM. Toxicity, biodistribution, and ex vivo MRI detection of intravenously injected cationized ferritin. Magn Reson Med. 2013;69:853–861. [PubMed: 22570266]

24. Charlton JB, Baldelomar EJ, deRonde KA, et al. Nephron loss detected by MRI following neonatal acute kidney injury in rabbits. Pediatr Res. 2020;87:1185–1192. [PubMed: 31805577]
25. Danon D, Goldstein L, Marikovsky Y, et al. Use of cationized ferritin as a label of negative charges on cell surfaces. J Ultrastruct Res. 1972;38:500–510. [PubMed: 4111070]
26. Baldelomar EJ, Charlton JR, Beeman SC, et al. Measuring rat kidney glomerular number and size in vivo with MRI. Am J Physiol Renal Physiol. 2018;314:F399–F406. [PubMed: 29092847]
27. Beeman SC, Zhang M, Gubhaju L, et al. Measuring glomerular number and size in perfused kidneys using MRI. Am J Physiol Renal Physiol. 2011;300. F1454–1457. [PubMed: 21411479]
28. Baldelomar EJ, Charlton JR, Beeman SC, et al. Phenotyping by magnetic resonance imaging nondestructively measures glomerular number and volume distribution in mice with and without nephron reduction. Kidney Int. 2016;89:498–505. [PubMed: 26535998]
29. Baldelomar EJ, Charlton JR, deRonde KA, et al. In vivo measurements of kidney glomerular number and size in healthy and Os(/+) mice using MRI. Am J Physiol Renal Physiol. 2019;317:F865–F873. [PubMed: 31339774]
30. Beeman SC, Cullen-McEwen LA, Puelles VG, et al. MRI-based glomerular morphology and pathology in whole human kidneys. Am J Physiol Renal Physiol. 2014;306:F1381–F1390. [PubMed: 24647716]
31. Forbes MS, Thornhill BA, Chevalier RL. Proximal tubular injury and rapid formation of atubular glomeruli in mice with unilateral ureteral obstruction: a new look at an old model. Am J Physiol Renal Physiol. 2011;301:F110–F117. [PubMed: 21429968]
32. Najafian B, Crosson JT, Kim Y, et al. Glomerulotubular junction abnormalities are associated with proteinuria in type 1 diabetes. J Am Soc Nephrol. 2006;17:S53–S60. [PubMed: 16565248]
33. Najafian B, Kim Y, Crosson JT, et al. Atubular glomeruli and glomerulotubular junction abnormalities in diabetic nephropathy. J Am Soc Nephrol. 2003;14:908–917. [PubMed: 12660325]
34. Chevalier RL, Forbes MS. Generation and evolution of atubular glomeruli in the progression of renal disorders. J Am Soc Nephrol. 2008;19:197–206. [PubMed: 18199796]
35. White KE, Marshall SM, Bilous RW. Prevalence of atubular glomeruli in type 2 diabetic patients with nephropathy. Nephrol Dial Transplant. 2008;23:3539–3545. [PubMed: 18558622]
36. Marcussen N, Christensen S, Petersen JS, et al. Atubular glomeruli, renal function and hypertrophic response in rats with chronic lithium nephropathy. Virchows Arch A Pathol Anat Histopathol. 1991;419:281–289. [PubMed: 1949611]
37. Landau SI, Guo X, Velazquez H, et al. Regulated necrosis and failed repair in cisplatin-induced chronic kidney disease. Kidney Int. 2019;95:797–814. [PubMed: 30904067]
38. Marcussen N Atubular glomeruli in cisplatin-induced chronic interstitial nephropathy. An experimental stereological investigation. APMIS. 1990;98:1087–1097. [PubMed: 2282204]
39. Chen HH, Waghorn PA, Wei L, et al. Molecular imaging of oxidized collagen quantifies pulmonary and hepatic fibrogenesis. JCI Insight. 2017;2:e91506.
40. Montesi SB, Desogere P, Fuchs BC, et al. Molecular imaging of fibrosis: recent advances and future directions. J Clin Invest. 2019;129:24–33. [PubMed: 30601139]
41. Parvin NB, Charlton JR, Baldelomar EJ, et al. Mapping vascular and glomerular pathology in a rabbit model of neonatal acute kidney injury using MRI. Anat Rec. 2020;303:2716–2728.
42. Yang HC, Zuo Y, Fogo AB. Models of chronic kidney disease. Drug Disc Today Dis Models. 2010;7:13–19.
43. Jamison RL. Intrarenal heterogeneity. The case for two functionally dissimilar populations of nephrons in the mammalian kidney. Am J Med. 1973;54:281–289. [PubMed: 4571744]
44. Bowman W On the structure and use of the malpighian bodies of the kidney, with observations of the circulation through that gland. Phil Trans Roy Soc London. 1842;132:57–80.
45. Kriz W [The architectonic and functional structure of the rat kidney]. Z Zellforsch Mikrosk Anat. 1967;82:495–535 [in German]. [PubMed: 4881295]
46. Hanssen OE. The relationship between glomerular filtration and length of the proximal convoluted tubules in mice. Acta Pathol Microbiol Scand. 1961;53:265–279. [PubMed: 13904471]
47. Weisser F, Lacy FB, Weber H, et al. Renal function in the chinchilla. Am J Physiol. 1970;219:1706–1713. [PubMed: 5485688]

48. de Rouffignac C, Morel F. Micropuncture study of water, electrolytes, and urea movements along the loops of henle in psammomys. J Clin Invest. 1969;48:474–486. [PubMed: 5773086]

49. Schindelin J, Arganda-Carreras I, Frise E, et al. Fiji: an open-source platform for biological-image analysis. Nat Methods. 2012;9:676–682. [PubMed: 22743772]

50. Xu Y, Wu T, Gao F, et al. Improved small blob detection in 3D images using jointly constrained deep learning and Hessian analysis. Sci Reports. 2020;10:326.

51. Ester M, Kriegel HP, Sander J, Xu X. A density-based algorithm for discovering clusters in large spatial databases with noise. In: Simoudis EH, Jiawei F, Fayya UM, eds. Proceedings of the Second International Conference on Knowledge Discovery and Data Mining (KDD-96). Palo Alto, CA: AAAI Press; 1996:226–231.

52. Geng Y, Zhang L, Fu B, et al. Mesenchymal stem cells ameliorate rhabdomyolysis-induced acute kidney injury via the activation of M2 macrophages. Stem Cell Res Ther. 2014;5:80. [PubMed: 24961539]

53. Forbes MS, Thornhill BA, Minor JJ, et al. Fight-or-flight: murine unilateral ureteral obstruction causes extensive proximal tubular degeneration, collecting duct dilatation, and minimal fibrosis. Am J Physiol Renal Physiol. 2012;303:F120–F129. [PubMed: 22535799]

54. Forbes MS, Thornhill BA, Galarreta CI, et al. Chronic unilateral ureteral obstruction in the neonatal mouse delays maturation of both kidneys and leads to late formation of atubular glomeruli. Am J Physiol Renal Physiol. 2013;305:F1736–F1746. [PubMed: 24107422]

55. Galarreta CI, Grantham JJ, Forbes MS, et al. Tubular obstruction leads to progressive proximal tubular injury and atubular glomeruli in polycystic kidney disease. Am J Pathol. 2014;184:1957–1966. [PubMed: 24815352]

56. Chong CD, Gaw N, Fu Y, et al. Migraine classification using magnetic resonance imaging resting-state functional connectivity data. Cephalalgia. 2017;37:828–844. [PubMed: 27306407]

57. Schwedt TJ, Si B, Li J, et al. Migraine subclassification via a data-driven automated approach using multimodality factor mixture modeling of brain structure measurements. Headache. 2017;57:1051–1064. [PubMed: 28627714]

58. Scindia Y, Dey P, Thirunagari A, et al. Hepcidin mitigates renal ischemia-reperfusion injury by modulating systemic iron homeostasis. J Am Soc Nephrol. 2015;26:2800–2814. [PubMed: 25788528]

59. Cook JD, Torrance JD, Bothwell TH. Tissue iron stores. New York, NY: Churchill Livingstone; 1980.

60. Aslan B, Zech G. Statistical energy as a tool for binning-free, multivariate goodness-of-fit tests, two-sample comparison and unfolding. Nucl Instrum Methods Physics Res A Accelerators Spectrom Detectors Assoc Equip. 2005;537:626–636.

Translational Statement

Acute kidney injury (AKI) is common in hospitalized patients. Many of the patients who experience AKI develop chronic kidney disease (CKD). However, it is difficult using clinically available tools to predict who will develop CKD and when. Cationic ferritin–enhanced magnetic resonance imaging (CFE-MRI) provides several measurements of functional glomeruli in preclinical studies. CFE-MRI has the potential to be translated to use in humans to detect changes in the kidney after AKI and predict which patients may develop CKD. The next steps toward translation will include *in vivo* tracking of glomerular fate in preclinical models of AKI to CKD and assessing the toxicity of CF in repeated doses.

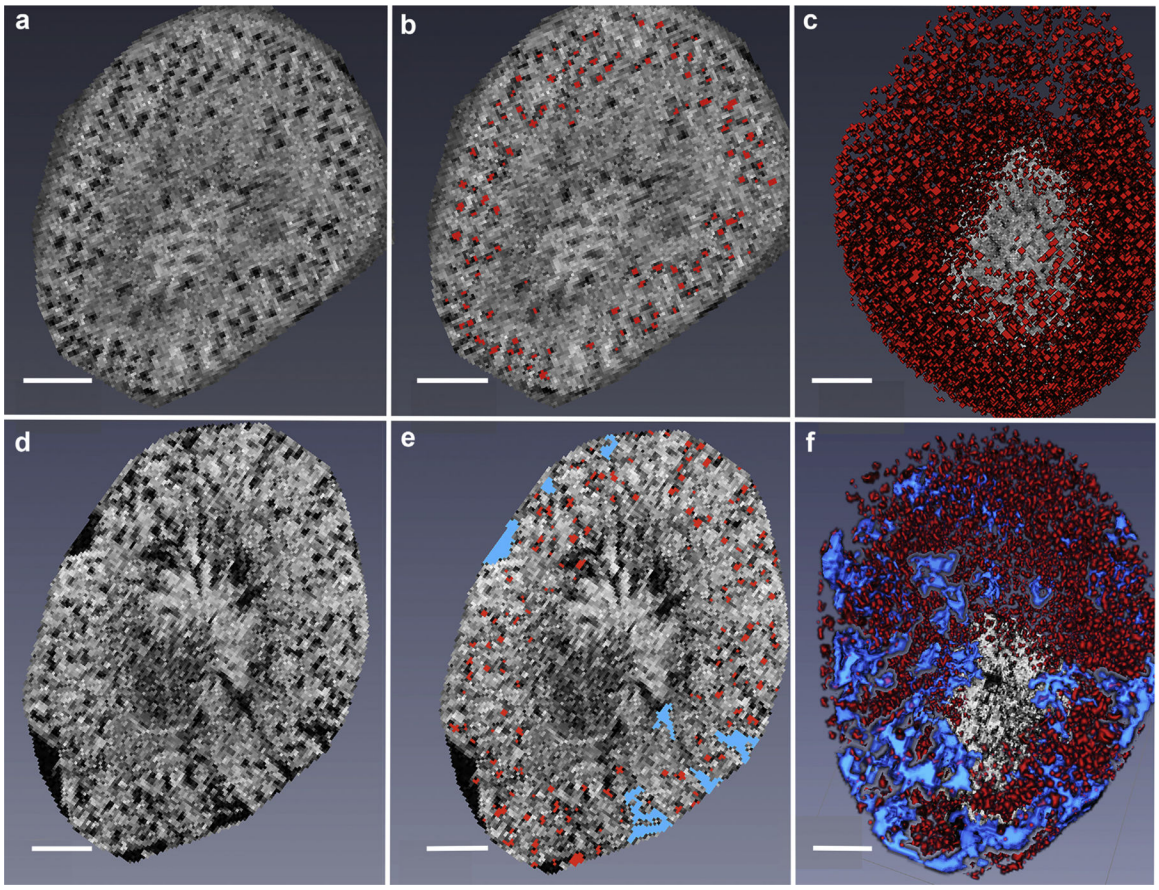

Figure 1 |. Gradient-echo magnetic resonance images of cationic-ferritin (CF)-labeled kidneys from healthy control mice compared with those with folic acid–induced chronic kidney disease (CKD).

(**a–c**) In the healthy kidney, (**a**) the glomeruli are visualized as distinct black dots in this representative 2-dimensional (2D) image. (**b**) Identified glomeruli are highlighted in red and (**c**) reconstructed in 3 dimensions. (**d–f**) In the CKD model, the black cortical wedge-shaped areas in the magnetic resonance images are termed “cortical lesions,” and within these black areas, the glomeruli are clustered together without attached tubules. (**d**) These glomeruli are too close to discriminate their individual size. (**e**) The cortical lesions are highlighted in blue. (**f**) As demonstrated in the 3-dimensional (3D) reconstruction, the cortical lesions (highlighted in blue) were observed throughout the kidney. The 3D reconstruction of the CKD kidney makes the number, size and extend of the lesions easier to appreciate than in the 2D slice. Not every glomerulus is labeled in red in the single 2D sections represented in (**b,d**). This is because the mask floats above the image, and the center of the glomerulus may have been identified in the 2D section above or below this representative slice. Bar = 1 mm. To optimize viewing of this image, please see the online version of this article at www.kidney-international.org.

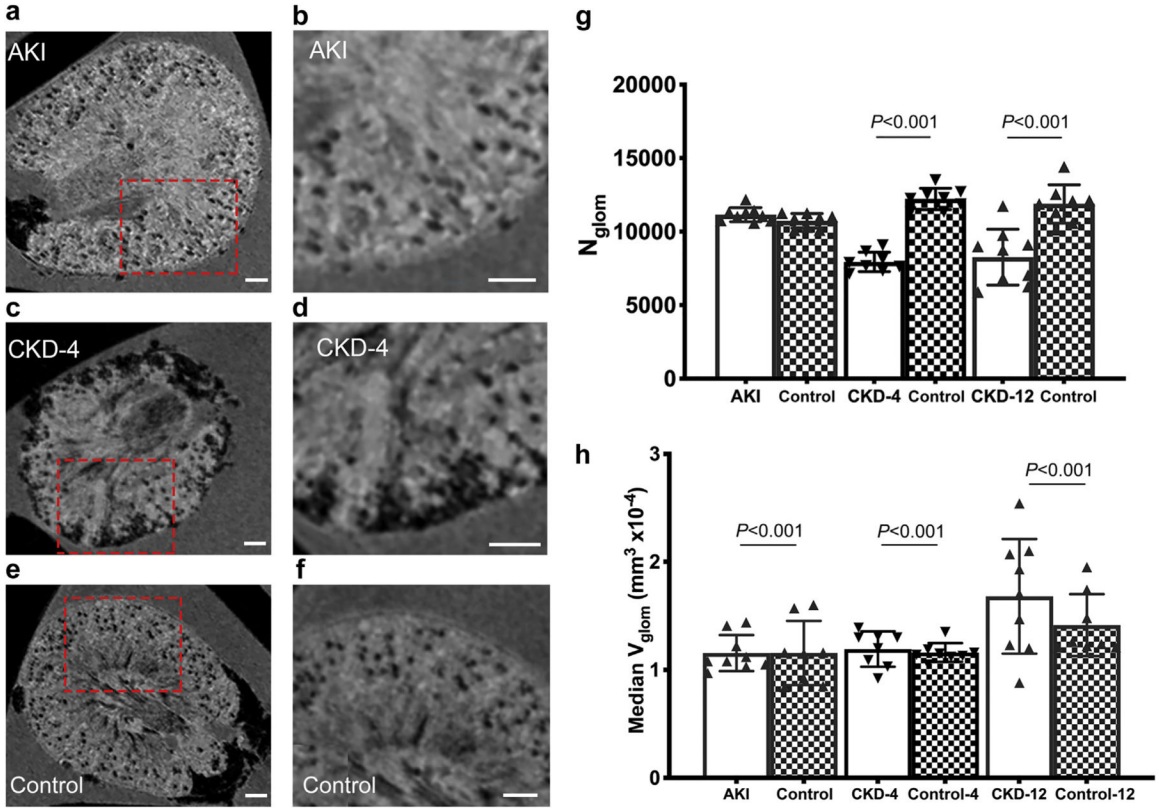

Figure 2 |. Cationic ferritin–enhanced magnetic resonance imaging (CFE-MRI) characteristics of the transition from acute kidney injury (AKI) to chronic kidney disease (CKD).

(**a–f**) Representative magnetic resonance images of mouse kidneys from AKI (**a,b**), CKD-4 (**c,d**), and control (**e,f**) groups. The red boxes in (**a,c,e**) outline the area magnified in (**b d,f**), respectively. (**g**) Glomerular number from CFE-MRI, where there are significantly fewer glomeruli in the CKD-4 and CKD-12 compared with controls. (**h**) Apparent glomerular volume is displayed as the median aV_{glom} using all of the data from each kidney. The median aV_{glom} is greater in the AKI, CKD-4, and CKD-12 groups compared with age-matched controls. Glomerular volume increases with aging as well. CKD-4, CKD 4 weeks after injury; CKD-12, CKD 12 weeks after injury. To optimize viewing of this image, please see the online version of this article at www.kidney-international.org.

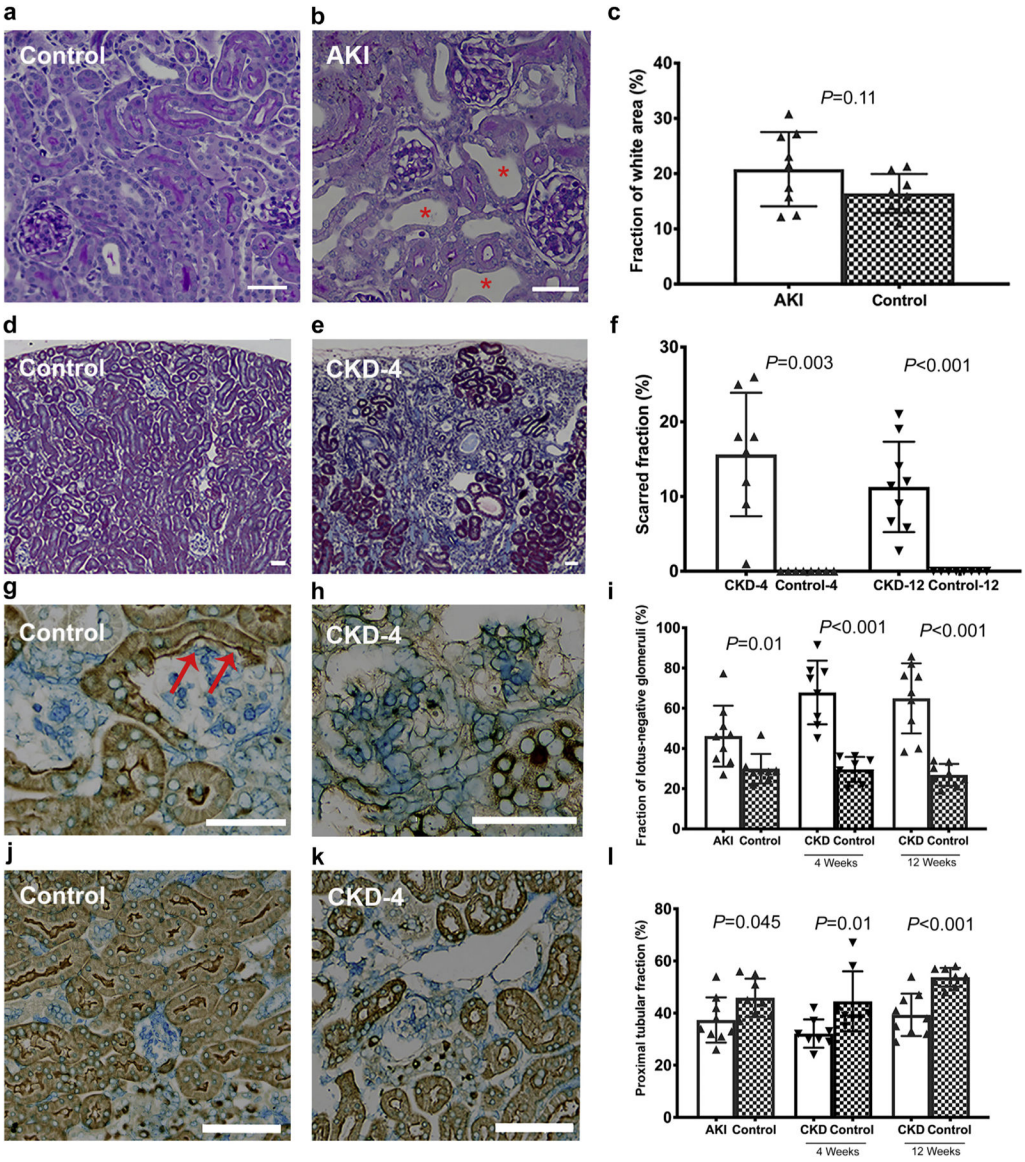

Figure 3 |. Histological characteristics of the transition from acute kidney injury (AKI) to chronic kidney disease (CKD).

(**a,b**) Representative tubular dilation in AKI group compared with the controls, where areas of tubular dilation were frequent in the AKI group (**b**; red *). (**c**) The quantification of the percentage of white space. Scarred area (**d–f**) was assessed by trichrome stain in the CKD-4 and CKD-12 groups. (**e**) The kidneys in the CKD-4 and CKD-12 groups were smaller and had cortical wedge-shaped lesions. These scarred areas contained many atrophic tubules and lotus-negative glomeruli (**h**). (**g–i**) Lotus-negative glomeruli and (**j–l**) proximal tubular fraction were assessed on lotus lectin stained kidneys. (**g**) A healthy glomerulus in a control animal where the glomerulus is connected to the tubule. The red arrows highlight the parietal cells marked as lotus-positive signifying an intact glomerulotubular junction. (**j–l**) Proximal tubular content was reduced in the CKD-12 group. Bars in the histologic sections = 50 μm. *P* values < 0.002 are considered significant. CKD-4, CKD 4 weeks after injury; CKD-12,

CKD 12 weeks after injury. To optimize viewing of this image, please see the online version of this article at www.kidney-international.org.

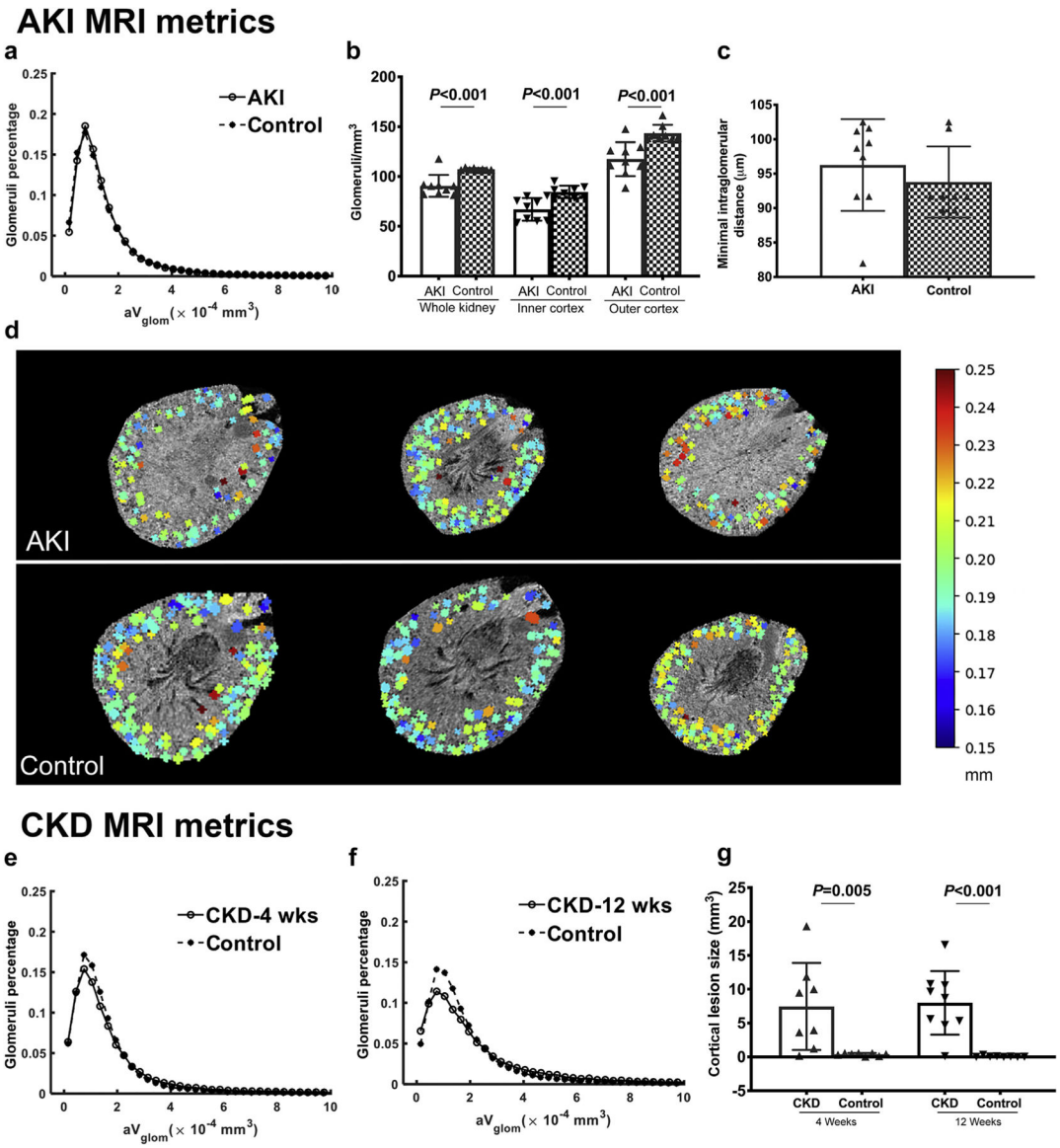

Figure 4 |. Development of magnetic resonance imaging biomarkers for acute kidney injury (AKI) and chronic kidney disease (CKD) time points.

(**a**) Cationic ferritin–enhanced MRI was used to measure the size of each glomerulus and the distribution of glomerular volumes (aV_{glom}). At the AKI time point, tubular dilation was common. Therefore, distance between glomeruli (**b**) and glomerular density (**c**) in the inner and outer cortex were used as biomarkers of AKI. Interglomerular distance was coded to a color scale (millimeters) and mapped to the magnetic resonance images. Representative images of the kidneys with AKI and controls with color overlay are seen in (**d**). The distribution of aV_{glom} in the CKD-4 (**e**) and CKD-12 groups (**f**) were different from controls. CKD-specific MRI biomarkers of cortical lesions size, number, and percentage of the kidney were developed for the cortical lesions. (**g**) Cortical lesion size was larger in both CKD-4 and CKD-12 compared with controls. CKD-4, CKD 4 weeks after injury; CKD-12, CKD 12 weeks after injury. To optimize viewing of this image, please see the online version of this article at www.kidney-international.org.

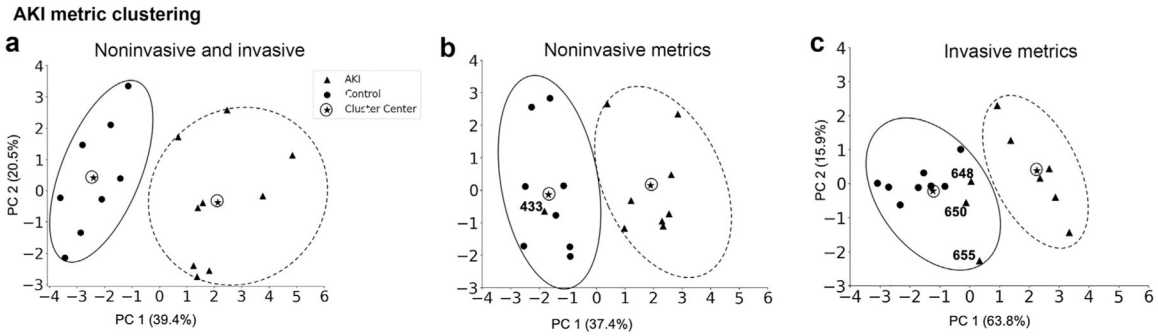

Figure 5 |. Clustering analysis of the acute kidney injury (AKI) group.

In combination, the invasive and noninvasive metrics (**a**) discriminate the AKI from the control group and the heterogeneity of each group is visible by the size of the circle surrounding the individual data points. A single animal was misclassified by the noninvasive (**b**) and 3 animals by the invasive (**c**) metrics. Extensive variability in the AKI group is captured in both the noninvasive and invasive cluster analysis.

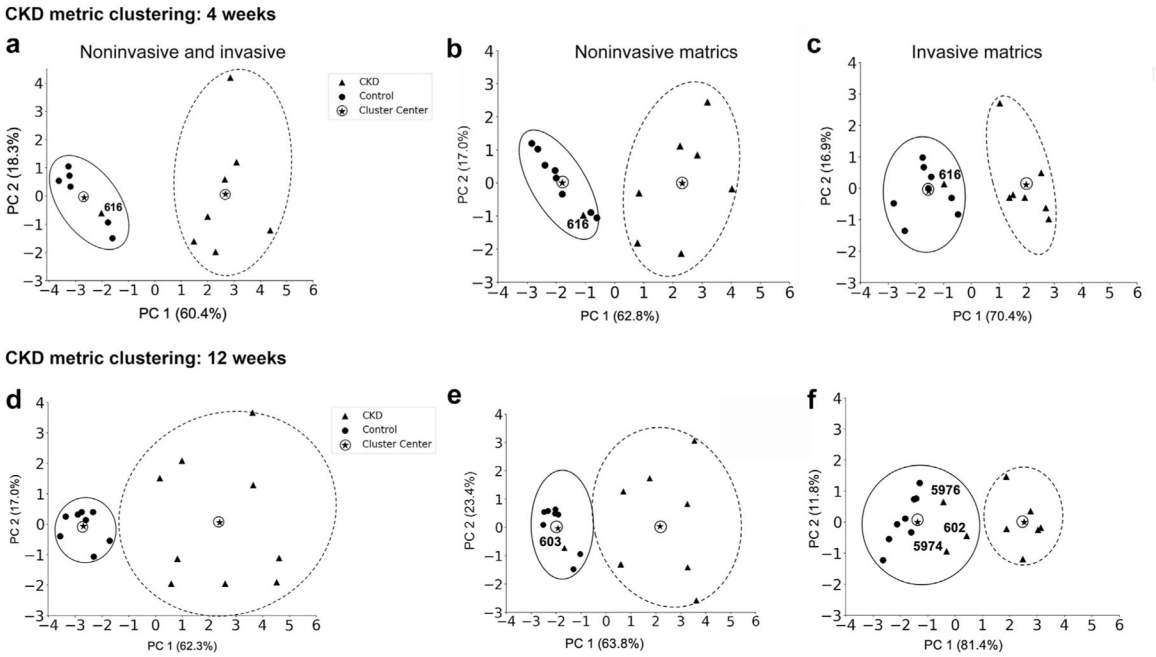

Figure 6 |. Clustering analysis of the chronic kidney disease (CKD)-4 and CKD-12 groups.
The combination of noninvasive and invasive metrics was able to discriminate the CKD groups from controls: (**a**) CKD-4 and (**d**) CKD-12. In the CKD-4 group, the same animal was misclassified by each of the 3 clustering analyses: (**a**) combination of noninvasive and invasive, (**b**) noninvasive, and (**c**) invasive, suggesting that this animal had a very mild AKI or was truly a control. At CKD-12, significant heterogeneity was demonstrated in the CKD-12 group compared with the controls when using a combination of invasive and noninvasive metric. One animal was misclassified in both the noninvasive metrics (**e**), and 3 animals were misclassified by invasive (**f**) metrics. CKD-4, CKD 4 weeks after injury; CKD-12, CKD 12 weeks after injury.

Table 1 |

Summary of MRI and histologic results

AKI	Control	*P*	Test	CKD-4	Control	*P*	CKD-12	Control	*P*	Test
Kidney volume (mm^3)										
206 ± 22	168 ± 17	0.001	*t*	143 ± 23	199 ± 25	<0.001	151 ± 38	212 ± 24	0.001	*t*
N_{glom}										
11,148 ± 475	10728 ± 490	0.09	*t*	7941 ± 659	12,219 ± 727	<0.001	8262 ± 1903	11,878 ± 1307	<0.001	*t*
aV_{glom} ($\times 10^{-4} mm^3$)										
1.12 (0.69–1.84)	1.10 (0.65–1.87)	<0.001	MW	1.26 (0.72–2.25)	1.17 (0.71–1.86)	4.2e-97	1.59 (0.83–3.02)	1.37 (0.81–2.29)	3.8e-168	MW
Lotus-negative glomeruli (%)										
46 (35–55)	29 (26–30)	0.01	MW	71 (53–79)	31 (23–35)	<0.001	68 (47–79)	26 (22–33)	<0.001	MW
Proximal tubule fraction (%)										
37 ± 8	46 ± 7	0.046	*t*	32 ± 5	45 ± 12	0.02	39 ± 8	54 ± 4	<0.001	*t*
AKI only							**CKD only**			
AKI	**Control**	***P***	**Test**	**CKD-4**	**Control**	***P***	**CKD-12**	**Control**	***P***	**Test**
Interglomerular distance (μm)							**Cortical lesion (#)**			
202.1 ± 0.65	202.4 ± 0.68	0.61	*t*	105 (22–155)	0.5 (0–2)	0.001	92 (26–176)	0 (0–1)	<0.001	MW
Minimal distance (mm)							**Cortical lesion size (mm^3)**			
98.7 (91.7c-101.4)	91.7 (90.2–99.1)	0.35	MW	6.7 (1.8–11.4)	0.4 (0.2–0.6)	<0.0047	8.7 (4.0–12.8)	0.03 (0–0.1)	<0.001	MW
Glomerular density (glomeruli/mm^3)							**Cortical lesion/kidney volume (%)**			
92.0 (75.0–106.5)	111.4 (94.4–123.5)	<0.001	MW	5.4 (1.3–8.2)	0.2 (0.1–0.3)	0.003	6.8 (2.4–9.8)	0.02 (0.0–0.2)	<0.001	MW
White space (%)							**Scarred area by trichrome (%)**			
21 ± 7	16 ± 4	0.11	*t*	17 (10–23)	0 (0–0)	<0.001	11 (6–17)	0 (0–0)	<0.0001	MW

AKI, acute kidney injury; CKD, chronic kidney disease; CKD-4, CKD 4 weeks after injury; CKD-12, CKD 12 weeks after injury; MRI, magnetic resonance imaging; MW, Mann–Whitney test; *t*, *t* test.

Table 2 |

Invasive and noninvasive metrics assessed in the AKI and CKD groups

	AKI		CKD-4 and CKD-12	
Invasive metrics	Kidney weight Kidney weight/body weight PT fraction-atubular glomeruli (%)	AKI score Tubular dilation (%)	Kidney weight Kidney weight/body weight PT fraction Atubular glomeruli (%)	Scarred area (%)
Noninvasive metrics	Body weight Kidney volume	N_{glom} $aV_{glom:}$ Median Mean Interglomerular distance: Minimum Mean Glomerular density: Whole kidney Inner cortex Outer cortex	Body weight Kidney volume	N_{glom} $aV_{glom:}$ Median Mean Cortical lesions: Number Volume LV/KV

AKI, acute kidney injury; aV_{glom}, apparent glomerular volume; CKD-4, CKD 4 weeks after injury; CKD-12, CKD 12 weeks after injury; LV, lesion volume; N_{glom}, glomerular number; PT, proximal tubule.